Optics Letters

Temporal resolution of ultrafast compressive imaging using a single-chirped optical probe

Haocheng Tang,[1] Miguel Marquez,[2] Ting Men,[1] Yaodan Hu,[1] Weiqi Tang,[1] Jinyang Liang,[2] and Zhengyan Li[1,3,*]

[1]School of Optical and Electronic Information and Wuhan National Laboratory of Optoelectronics, Huazhong University of Science and Technology, Wuhan 430074, China
[2]Centre Énergie Matériaux Télécommunications, Institut National de la Recherche Scientifique, Université du Québec, Varennes, Québec J3X1P7, Canada
[3]Optics Valley Laboratory, Wuhan 430074, China
*zhengyanli@hust.edu.cn

Received 5 September 2023; revised 14 October 2023; accepted 24 October 2023; posted 24 October 2023; published 15 November 2023

Ultrafast compressive imaging captures three-dimensional spatiotemporal information of transient events in a single shot. When a single-chirped optical probe is applied, the temporal information is obtained from the probe modulated in amplitude or phase using a direct frequency–time mapping method. Here, we extend the analysis of the temporal resolution of conventional one-dimensional ultrafast measurement techniques such as spectral interferometry to that in three-dimensional ultrafast compressive imaging. In this way, both the amplitude and phase of the probe are necessary for a full Fourier transform method, which obtains temporal information with an improved resolution determined by probe spectral bandwidth. The improved temporal resolution potentially enables ultrafast compressive imaging with an effective imaging speed at the quadrillion-frames-per-second level.

https://doi.org/10.1364/OL.505260

Single-shot ultrafast imaging captures transient dynamic scenes of matter using one or multiple laser pulses, equivalent to taking movie frames with a temporal resolution of femtoseconds. The multi-probe geometry uses a few probing laser pulses with different time delays, offering snapshots of ultrafast events with clearly defined frame rate and temporal resolution [1–6]. In the single-probe geometry, the time-dependent dynamics is continuously recorded by either a streak camera in the time domain [7,8] or a chirped probe pulse in the frequency domain.

The idea of single-chirped probe has been early demonstrated in single-shot spectral interferometry utilizing phase modulation on the probe [9–11]. There are two approaches to resolving time-dependent information. One takes advantage of the linear chirp of the probe pulse, and the temporal information is directly mapped onto the spectrum of the probe [9]. However, the direct frequency–time mapping scheme has a temporal resolution degraded by the excessive chirp of the probe [10]. To solve this problem, the other approach carefully characterizes the probe phase, so a full Fourier transform scheme reveals the probe modulation in the temporal domain with an enhanced temporal resolution only determined by the probe spectral bandwidth [12,13].

Analogous to conventional single-shot spectral interferometry, the spatiotemporal information is obtained from the modulated spectrum of the probe using the direct frequency–time mapping approach under the framework of compressive imaging [14,15]. In this case, imaging frame rates up to multi-trillion frames per second have been reported by simply calculating the inverse of the reconstructed frame temporal interval [14,15]; however such a definition of the frame rate ignores the temporal resolution limit of the direct frequency–time mapping scheme [10]. Recently we have experimentally demonstrated compressive imaging of both phase and amplitude spatial–spectral profiles simultaneously [16], allowing the full Fourier transform scheme to be applied for temporal information with improved resolution.

Here we extend the analysis of temporal resolution from one-dimensional ultrafast dynamics measurement to that in three-dimensional ultrafast compressive imaging, using a single-chirped probe pulse. Compared to previous experimental demonstration of ultrafast compressive imaging based on the full Fourier transform scheme [16], we focus on theoretical analysis and numerical simulations to prove the concept without being interfered by practical experimental errors and technical challenges. By comparing two different approaches for obtaining temporal information in the context of three-dimensional ultrafast compressive imaging, it is shown that phase information is critical to perform the full Fourier transform procedure, yielding an improved temporal resolution compared to the direct frequency–time mapping case.

Compared to previous one-dimensional studies of the direct frequency–time mapping and full Fourier transform schemes applied to temporally phase-modulated probe pulses in spectral interferometry [10,12], amplitude modulation is more common for ultrafast compressive imaging. Unfortunately, an analytical formula of the temporal resolution for the amplitude modulation case is absent in literature. So we start with a one-dimensional analysis of a chirped probe laser pulse experiencing a transient dynamic event modulating the probe amplitude in time, i.e., a linearly chirped probe pulse $E_{\mathrm{pr}}(t)$ is modulated in amplitude by a "Gaussian" transient event $f(t,\tau) = \delta\exp[-(t-\tau)^2/\Delta t^2]$ with a temporal modulation depth

δ, time delay τ, and temporal duration Δt, in the way of $E'_{\mathrm{pr}}(t,\tau) = E_{\mathrm{pr}}(t)[1 - f(t,\tau)]$. The incident probe pulse in the frequency domain is $E_{\mathrm{pr}}(\omega) = E_0 \exp(-\omega^2/\Omega^2 + i\beta_2\omega^2)$, where Ω is the frequency bandwidth and β_2 is the group velocity dispersion. In the direct frequency–time mapping scheme, the transient event is extracted from the measured signal in the frequency domain $f'(t,\tau) = 1 - |E'_{\mathrm{pr}}(\alpha\omega,\tau)/E_{\mathrm{pr}}(\alpha\omega)|$, where $\alpha = 2\beta_2(1 + \beta_2^{-2}\Omega^{-4})$ is the linear chirp coefficient. Without a loss of generality, we study the reconstructed event $f(t,\tau)$ at $\tau = 0$ and assume a small modulation depth ($\delta \ll 1$), so

$$f'(t,0) = \delta(\zeta^2 + \eta^2)^{1/4} \exp[-(\zeta - 2\varepsilon\eta)(t/\Delta t)^2] \cdot \cos[(\eta + 2\varepsilon\zeta)(t/\Delta t)^2 - \theta], \quad (1)$$

where $\epsilon = \frac{1}{\sqrt{1+\beta_2^2\Omega^4}}$, $\zeta = \frac{1+\frac{4}{(\Omega\Delta t)^2}}{1+\frac{8}{(\Omega\Delta t)^2}+\frac{16(1+\beta_2^2\Omega^4)}{(\Omega\Delta t)^4}}$, $\eta = \frac{4\beta_2/(\Delta t)^2}{1+\frac{8}{(\Omega\Delta t)^2}+\frac{16(1+\beta_2^2\Omega^4)}{(\Omega\Delta t)^4}}$, and $\theta = \frac{1}{2}\arctan\left(\frac{\eta}{\zeta}\right)$.

The reconstructed transient event $f'(t,0)$ differs from the original one in three aspects. First, the reconstructed amplitude modulation depth is always smaller than δ by a factor of $[(\zeta^2 + \eta^2)^{1/4}\cos\theta]^{-1} > 1$ [Fig. 1(a)], and the underestimation of the modulation depth increases as Δt decreases. Second, the reconstructed temporal duration of the transient event is broadened to $\Delta t(\zeta - 2\epsilon\eta)^{1/2}$, and the temporal broadening of the reconstruction increases for fast evolution with small Δt [Fig. 1(b)]. Third, the $\cos[(\eta + 2\epsilon\zeta)(t/\Delta t)^2 - \theta]$ term shows an oscillating behavior of the reconstructed temporal profile. The ratio of the broadened temporal duration to the effective oscillation period $[(\eta + 2\epsilon\zeta)/(\zeta - 2\epsilon\eta)]^{1/2}$ is beyond 1 when Δt is small, and the reconstruction is harmed by the oscillation artifacts [Fig. 1(c)].

Thus all three types of discrepancy of the reconstruction become significant for fast transient events with small Δt and for the probe pulse with extensive dispersion $\beta_2\Omega^2$. So we define a dispersion-dependent temporal resolution of the direct frequency–time mapping scheme

$$t_{\mathrm{res}} = \left(\frac{4}{\Omega^2}\sqrt{1 + \beta_2^2\Omega^4}\right)^{1/2} \quad (2)$$

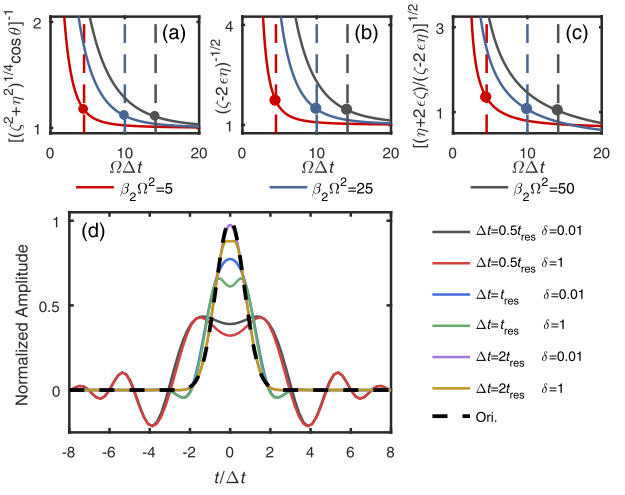

Fig. 1. Parametric study for the reconstruction with direct frequency–time mapping scheme. (a)–(c) Three critical ratios versus transient event duration $\Omega\Delta t$ at different dispersion $\beta_2\Omega^2$. (d) Comparison between the reconstructed temporal modulation profiles using direct frequency–time mapping and the original one with different parameters.

as the minimum duration of a transient event that can be reconstructed without significant deformation. Quantitatively, this value results in $\zeta = 2$, yielding a nearly $\sqrt{2}$-fold broadening since $2\epsilon\eta$ is small especially when the dispersion is large. For different normalized probe dispersion $\beta_2\Omega^2$, the temporal resolution t_{res} [dots shown in Figs. 1(a)–1(c)] defines the characteristic time of the transient event lower than which the reconstruction is degraded. In addition, the effective frame number $N = (1 + \beta_2^2\Omega^4)^{1/4}$ is obtained by dividing the chirped probe pulse duration by the temporal resolution, equal to the square root of the pulse stretch ratio.

Figure 1(d) shows temporal profile reconstructions of a transient event (black-dashed line) for different original temporal durations Δt and modulation depths δ using the direct frequency–time mapping method. In the simulations, $\beta_2\Omega^2$ is set to 48 so that $N = 7$ is an integer. When $\Delta t = 2t_{\mathrm{res}}$, the reconstructed temporal profiles are close to the original one (brown and purple lines), though the modulation depth is slightly underestimated for strong modulation (δ=1). The reconstructed temporal duration is broadened when $\Delta t = t_{\mathrm{res}}$ (blue and green lines), and the oscillating structure appears. Once the original temporal duration is smaller than the resolution limit, the reconstruction is ruined by significantly broadened oscillations (red and gray lines). It is worth mentioning that the case of phase modulation would exhibit similar features to the case of amplitude modulation. By comparing the reconstructed temporal profile of the transient event from a phase-modulated probe with the ground truth (data not shown) [12,13], the distortion is more sensitive to modulation depth δ, accounting for the self-phase modulation effect [17].

Now we extend discussions from one-dimensional temporal measurement to three-dimensional ultrafast compressive imaging using a chirped probe pulse. Chirped pulse-based ultrafast compressive imaging measures dynamic scenes by modulating the probe pulse in amplitude or phase by transient events, and the three-dimensional spectral–spatial intensity profile $I(x,y,\omega)$ is reconstructed using a coded aperture snapshot spectral imaging (CASSI) system which includes a coded aperture, an angular dispersive optics, and a two-dimensional detector [18,19]. Temporal information is obtained by either the direct frequency–time mapping scheme [14,15] or measuring the complete phase profile $\varphi(x,y,\omega)$ and calculating the spatiotemporal amplitude and phase profiles using a full Fourier transform scheme [16].

In the direct frequency–time mapping scheme, the probe pulse containing the dynamics scene is spatially coded by a random binary aperture. Spatial intensity profiles for different spectral components are sheared along one direction by angular dispersive optics such as a grating or a prism in experiments and summed up on the detector, yielding the raw two-dimensional CASSI snapshot. Finally, the CASSI reconstruction $I(x,y,\omega)$ is directly mapped to the time domain based on the probe chirp rate [Fig. 2(a)]. In the simulations, we assume a dynamic scene of a rotating fan as the ground truth (GT), including three petals A, B, and C with half angular $1/e$ widths of 19°, 25°, and 31°, respectively [Fig. 2(b)]. We choose the rotating fan as the "model" dynamic scene because the angular widths of fan petals in reconstructed image frames are broadened if the dynamic scene evolves faster than the temporal resolution, though implementing such a rotating fan as a "model" dynamic scene in experiments is technically challenging. We define a temporal gauge Δt describing the evolution rate of the dynamic scene which is fast enough to test the temporal resolution limit and even faster than previously measured dynamic scenes in experiments [14–16]. In

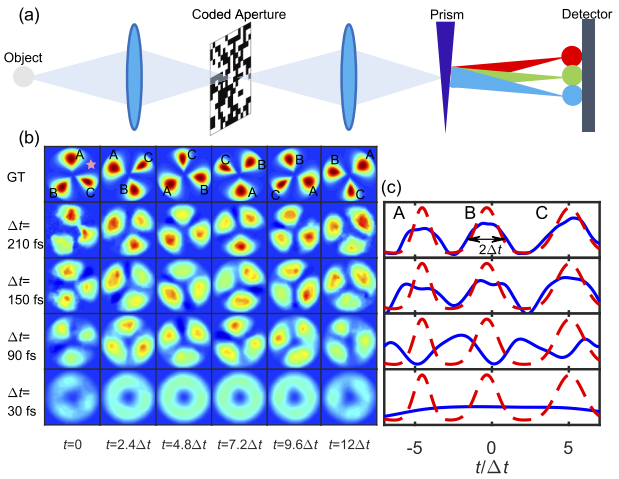

Fig. 2. Principle and simulation results of the direct frequency–time mapping scheme. (a) Schematic diagram of the data acquisition process. (b) Comparison between the reconstructed frame images and the GT at different Δt. (c) Comparison of the temporal profile at a specific spatial position between the reconstruction and the GT.

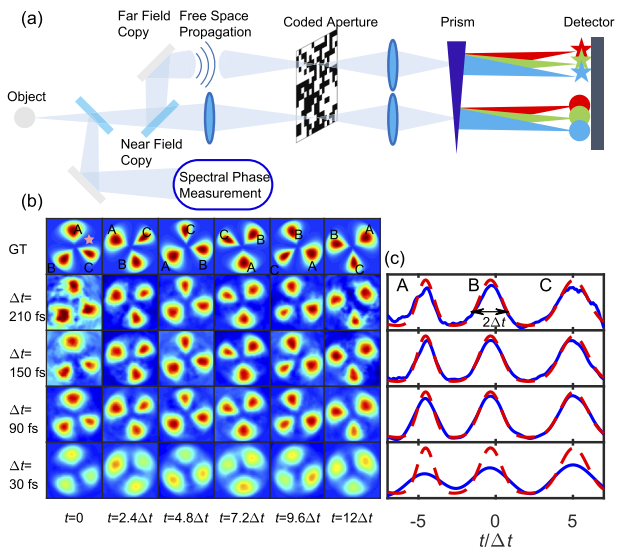

Fig. 3. Principle and simulation results of the full Fourier transform scheme. (a) Schematic diagram of the data acquisition process. (b) Comparison between the reconstructed frame images and the GT at different Δt. (c) Comparison of the temporal profile at a specific spatial position between the reconstruction and the GT.

simulations, Δt is the time during which the petals rotate for half angular $1/e$ width of petal B, e.g., 25°, and the rotation period is 14.4 Δt. The dynamic scene introduces an instantaneous temporal modulation to the amplitude of the temporally chirped probe pulse with a modulation depth of δ =0.5.

The characteristic time Δt of the petal rotation is varied to test the temporal resolving capability of the probe, which is chirped to 1470 fs from a 30 fs Fourier-limited duration pulse, determining t_{res} =210 fs according to Eq. (2). As Δt decreases, one may expect that the reconstructed dynamic scene is distorted when $\Delta t \sim t_{res}$, implying that the temporal resolution limit is reached. Figure 2(b) shows the reconstructed spatial modulation evolution histories for different Δt (i.e., 210, 150, 90, and 30 fs). Compared to the ground truth, the angular sizes of the reconstructed three petals are broadened for all rotation periods, thus the differences among them can hardly be resolved. In addition, the central angular positions of the reconstructed three petals for Δt = 90 fs are out of phase compared to the ground truth. For Δt = 30 fs, the three petals in the reconstruction are even indistinguishable. To further illustrate the temporal resolving capability, Fig. 2(c) lines out the temporal modulation of the probe at a specific spatial point shown as an asterisk mark in Fig. 2(b). For Δt =210 and 150 fs, the temporal duration of transient events, i.e., passing of three petals, is broadened. For Δt =90 and 30 fs, the reconstructions fail.

To improve the effective temporal resolution, an alternative full Fourier transform scheme is applied by utilizing the phase information of the probe. As shown in Fig. 3(a), the probe modulated by the dynamic scene is divided by a beam splitter into two copies. For the near-field copy, the dynamic scene is imaged to the coded aperture of the CASSI system. For the far-field copy, the probe propagates in free space for enough distance, and the diffraction pattern on the coded aperture is captured by the CASSI system. Experimental details are available in Ref. [16]. The spatial–spectral intensity profiles at both near and far fields are reconstructed using the standard CASSI technique. Based on the far- and near-field intensity profiles, a two-dimensional phase retrieval scheme is applied to obtain the spectrally resolved wavefront information. Next the spectral phase information, which in experiments is independently measured in a separate optical path without significant spectral dispersion or spatial chirp before the far and near-field copies are separated, is implemented, and a full Fourier transform scheme yields the three-dimensional spatiotemporal profile $E(x, y, t)$ of the modulated probe pulse.

Figure 3(b) shows the three-petal dynamic scenes extracted from the relative modulations of the probe amplitude profiles at different times with different rotation periods. For Δt = {210, 150, 90} fs, the reconstructed petals retain their original shapes with negligible deformation. The petals are only broadened when Δt =30 fs, but their rotations are still in phase with the ground truth and remain distinguishable in terms of angular width. The temporal line-outs of the probe amplitude modulation for different petal rotation periods are plotted in Fig. 3(c). Even for a temporal feature as fast as Δt =90 fs [Fig. 3(c), the third row], the reconstruction quality is satisfactory though the feature duration is significantly lower than the temporal resolution t_{res} for the direct frequency–time mapping scheme. Only when the transient event duration Δt =30 fs is comparable to the Fourier-limited pulse duration of the probe which is only determined by the probe spectral bandwidth, the reconstructed temporal duration is broadened by 1.4 times [Fig. 3(c), the fourth row], which is also close to the broadening ratio in the direct frequency–time mapping scheme when the event duration is close to the temporal resolution determined by Eq. (2). Thus image distortions in Fig. 3 are predominantly due to the temporal resolution limit.

We quantitatively evaluate the reconstruction qualities of the spatiotemporal modulation on the probe laser by introducing a mean structural similarity (MSSIM) metric [20]. The MSSIM metric varies from 0 to 1, and a high value of MSSIM represents that the reconstructed dynamic scenes are close to the ground truth. Figure 4 shows MSSIM parameters for reconstructions of the rotating petals with different rotation periods,

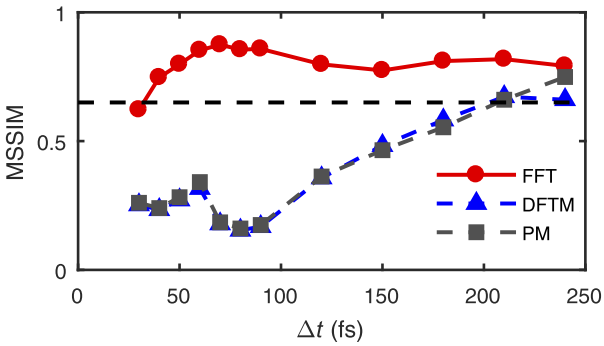

Fig. 4. MSSIM values of the three schemes for different Δt, FFT for the full Fourier transform approach, DFTM for the direct frequency–time mapping approach, and PM for the case of perfect mapping, a direct frequency–time mapping scheme without CASSI reconstruction.

using both the direct frequency–time mapping (DFTM) (blue) and the full Fourier transform (FFT) approaches (red). We have also directly mapped the calculated probe spectral–spatial intensity profile $I(x, y, \omega)$, rather than the CASSI reconstruction, to the time domain, yielding reconstructions of dynamics scenes denoted as "perfect mapping" (PM) (gray). MSSIM for the direct frequency–time mapping and the perfect mapping schemes are close, excluding the possibility that the CASSI reconstruction degrades the imaging reconstruction quality.

Furthermore, the MSSIM metric for the direct frequency–time mapping scheme are significantly lower than those for the full Fourier transform scheme. When $\Delta t = 210$ fs which equals to t_{res} in Eq. (2), the MSSIM values for both the direct mapping and the perfect mapping schemes are around 0.65 (Fig. 4, black-dashed line). In contrast, for the full Fourier transform scheme, a similar MSSIM value is obtained even when Δt is as small as 30 fs, similar to the Fourier-limited pulse duration of the probe. In this case, it is the probe spectral modulation instead of the probe chirp that encodes all necessary temporal information of transient events. So the probe spectral bandwidth sets the bandwidth limit of temporal measurements and determines the temporal resolution of the full Fourier transform scheme.

Finally, it is noted that we assume unlimited spatial resolutions in all simulations, in order to highlight the limiting effect of temporal resolution. Compared to ordinary imaging techniques whose spatial resolutions are determined by light wavelength and imaging numerical aperture, that of compressive imaging is further complicated by the pixel size of the coded aperture and the image reconstruction artifacts. In experiments, the coded aperture pixel size together with the imaging magnification can be optimized to reduce its degradation to the spatial resolution [16], thus even nanoscale spatial resolution can be achieved for compressive imaging [21]. On the other hand, novel reconstruction algorithms have been progressing to reduce artifacts and preserve the spatial resolution [22]. Therefore, our assumption of unlimited spatial resolution is valid and reasonable.

In conclusion, we have clarified temporal resolutions of different ultrafast compressive imaging implementations using a single-chirped optical probe. To decode temporal information of transient events from spectral modulations of the probe, the probe phase is necessary to conduct the full Fourier transform scheme, and a temporal resolution only determined by the probe spectral bandwidth can be obtained. Moreover, the full Fourier transform scheme provides both amplitude and phase modulations of the probe pulse, enabling complete characterization of optical properties, i.e., complex refractive index, of objects undergoing ultrafast evolution. Thanks to the temporal resolution of the full Fourier transform scheme which is as short as the inverse of the probe bandwidth, as well as nonlinear spectral broadening [23] and optical wave synthesis [24] techniques, ultrafast compressive imaging at a quadrillion effective frame rate is promising using an optical probe with a spectral bandwidth beyond one or more octaves.

Funding. National Key Research and Development Program of China (No. 2022YFB4601300); National Natural Science Foundation of China (No. 12275099, No. 52130504); Innovation Project of Optics Valley Laboratory (No. OVL2021ZD001); Innovation Fund of WNLO.

Disclosures. The authors declare no conflict of interests.

Data availability. Data underlying the results presented in this paper are not publicly available at this time but may be obtained from the authors upon reasonable request.

REFERENCES

1. X. Zeng, S. Zheng, Y. Cai, *et al.*, Adv. Photonics **2**, 056002 (2020).
2. A. Ehn, J. Bood, Z. Li, *et al.*, Light: Sci. Appl. **6**, e17045 (2017).
3. Q. Zhu, Y. Cai, X. Zeng, *et al.*, Opt. Express **30**, 27429 (2022).
4. C. Hu, Z. Du, M. Chen, *et al.*, Opt. Lett. **44**, 4419 (2019).
5. J. Moon, S. Yoon, Y. Lim, *et al.*, Opt. Express **28**, 4463 (2020).
6. K. Nakagawa, A. Iwasaki, Y. Oishi, *et al.*, Nat. Photonics **8**, 695 (2014).
7. L. Gao, J. Liang, C. Li, *et al.*, Nature **516**, 74 (2014).
8. J. Liang, L. Zhu, and L. V. Wang, Light: Sci. Appl. **7**, 42 (2018).
9. C. Y. Chien, B. La Fontaine, A. Desparois, *et al.*, Opt. Lett. **25**, 578 (2000).
10. J.-P. Geindre, P. Audebert, S. Rebibo, *et al.*, Opt. Lett. **26**, 1612 (2001).
11. N. H. Matlis, S. Reed, S. S. Bulanov, *et al.*, Nat. Phys. **2**, 749 (2006).
12. E. Tokunaga, A. Terasaki, and T. Kobayashi, J. Opt. Soc. Am. B **13**, 496 (1996).
13. K. Y. Kim, L. Alexeev, and H. M. Michberg, Appl. Phys. Lett. **81**, 4124 (2002).
14. Y. Lu, T. T. W. Wong, F. Chen, *et al.*, Phys. Rev. Lett. **122**, 193904 (2019).
15. P. Wang, J. Liang, and L. V. Wang, Nat. Commun. **11**, 2091 (2020).
16. H. Tang, T. Men, X. Liu, *et al.*, Light: Sci. Appl. **11**, 244 (2022).
17. R. H. Stolen and C. Lin, Phys. Rev. A **17**, 1448 (1978).
18. A. Wagadarikar, R. John, R. Willett, *et al.*, Appl. Opt. **47**, B44 (2008).
19. G. R. Arce, D. J. Brady, L. Carin, *et al.*, IEEE Signal Process. Mag. **31**, 105 (2014).
20. Z. Wang, A. C. Bovik, H. R. Sheikh, *et al.*, IEEE Trans. on Image Process. **13**, 600 (2004).
21. Y. He, Y. Yao, D. Qi, *et al.*, Adv. Photonics **5**, 026003 (2023).
22. X. Yuan, D. J. Brady, and A. K. Katsaggelos, IEEE Signal Process. Mag. **38**, 65 (2021).
23. J. M. Dudley, G. Genty, and S. Coen, Rev. Mod. Phys. **78**, 1135 (2006).
24. S.-W. Huang, G. Cirmi, J. Moses, *et al.*, J. Phys. B: At. Mol. Opt. Phys. **45**, 074009 (2012).